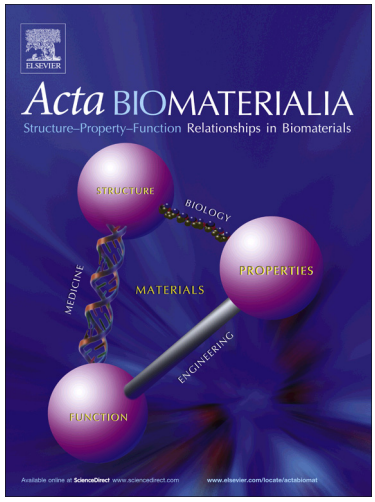

Full length article

New findings confirm the viscoelastic behaviour of the inter-lamellar matrix of the disc annulus fibrosus in radial and circumferential directions of loading

J. Tavakoli, J.J. Costi

PII: S1742-7061(18)30135-1
DOI: https://doi.org/10.1016/j.actbio.2018.03.015
Reference: ACTBIO 5357

To appear in: *Acta Biomaterialia*

Received Date: 18 December 2017
Revised Date: 13 February 2018
Accepted Date: 7 March 2018

Please cite this article as: Tavakoli, J., Costi, J.J., New findings confirm the viscoelastic behaviour of the inter-lamellar matrix of the disc annulus fibrosus in radial and circumferential directions of loading, *Acta Biomaterialia* (2018), doi: https://doi.org/10.1016/j.actbio.2018.03.015

New findings confirm the viscoelastic behaviour of the inter-lamellar matrix of the disc annulus fibrosus in radial and circumferential directions of loading.

Tavakoli J,[1] Costi JJ[1]

[1]Biomechanics and Implants Research Group, The Medical Device Research Institute, College of Science and Engineering, Flinders University, GPO Box 2100, Adelaide, South Australia 5001, Australia

Corresponding Author: John J Costi, john.costi@flinders.edu.au

Flinders University, GPO Box 2100, Adelaide, SA 5001 Australia

Abstract

While few studies have improved our understanding of composition and organization of elastic fibres in the inter-lamellar matrix (ILM), its clinical relevance is not fully understood. Moreover, no studies have measured the direct tensile and shear failure and viscoelastic properties of the ILM. Therefore, the aim of this study was, for the first time, to measure the viscoelastic and failure properties of the ILM in both the tension and shear directions of loading. Using an ovine model, isolated ILM samples were stretched to 40% of their initial length at three strain rates of 0.1%s^{-1} (slow), 1%s^{-1} (medium) and 10%s^{-1} (fast) and a ramp test to failure was performed at a strain rate of 10%s^{-1}. The findings from this study identified that the stiffness of the ILM was significantly larger at faster strain rates, and energy absorption significantly smaller, compared to slower strain rates, and the viscoelastic and failure properties were not significantly different under tension and shear loading. We found a strain rate dependent response of the ILM during dynamic loading, particularly at the fastest rate. The ILM demonstrated a significantly higher capability for energy absorption at slow strain rates compared to medium and fast strain rates. A significant increase in modulus was found in both loading directions and all strain rates, having a trend of larger modulus in tension and at faster strain rates. The finding of no significant difference in failure properties in both loading directions, was consistent with our previous ultra-structural studies that revealed a well-organized (±45°) elastic fibre orientation in the ILM. The results from this study can be used to develop and validate finite element models of the AF at the tissue scale, as well as providing new strategies for fabricating tissue engineered scaffolds.

Statement of significance

While few studies have improved our understanding of composition and organization of elastic fibres in the inter-lamellar matrix (ILM) of the annulus in the disc no studies have

measured the direct mechanical failure and viscoelastic properties of the ILM. The findings from this study identified that the stiffness of the ILM was significantly larger at faster strain rates, and energy absorption significantly smaller, compared to slower strain rates. The failure properties of the ILM were not significantly different under tension and shear.

Keywords:
Inter-lamellar matrix, Annulus fibrosus, viscoelastic property, failure property, material property, tension, shear

1. Introduction

With a unique hierarchical structure, the annulus fibrosus (AF) of the intervertebral disc is comprised of annular lamellae with alternating orientation of collagen fibres embedded in a proteoglycan-rich ground matrix [1]. The inter-lamellar matrix (ILM), with a thickness of approximately 20 μm, lies between lamellae and consists of collagen type IV, cells, several glycoproteins and matrix; however, elastic fibres were recognized as its main component [2-6]. Microstructural studies of the ILM revealed higher elastic fibre density relative to the intra-lamellar region [7-10], while further insight into ILM elastic fibre ultrastructure identified a dense and complex network of thick (diameter of 1-2 μm) and thin (0.1 μm diameter) fibres that were not randomly distributed [11].

The clinical relevance of the ILM is not fully understood. However, loss of structural boundaries between lamellae in scoliotic discs, which are more vulnerable to degeneration, along with evidence interpreting an increase of irregularity and interdigitating of lamellae structure with age, may show a correlation between the ILM disorganization and disc degeneration [12, 13]. Investigation of AF radial cohesion identified a complex hierarchy of interconnecting fibres in the ILM-lamella boundary that demonstrates the role of the ILM in

lamellae connectivity [14]. Furthermore, based on studies of AF delamination, tears, patterns of herniation of the whole disc and lamellae peel strength, it is likely that the ILM plays a role in providing AF structural integrity [15-18]. Therefore, failure of the ILM may contribute to the initial stages of herniation and disc degeneration [19-21]. Knowledge of the structure-function relationship in the ILM is crucial in identifying the loading conditions that contribute to AF delamination or increased risk of disc herniation. Development of clinical strategies including tissue engineering scaffold fabrication and herniation treatment requires a greater understanding of the ILM mechanical and structural properties.

In spite of recent progress identifying the ultrastructure of the ILM, there is limited knowledge on its mechanical role. The ILM shear strength has been found to increase with lamella thickness [22], and deform by up to 10 mm, having a mean (SD) peak shear strength of 0.03 (0.05) MPa during delamination [23]. Significantly different shear stress and strain distributions, with a trend of being greater in the lamella than across the ILM, were found in disc mechanical modelling when inter-lamellar connectivity was considered [24, 25]. Also higher strain was reported in the ILM compared to the intra-lamellar region in bovine discs [26].

In the radial direction, the ILM structural connectivity was discussed, yet the mechanical properties of the ILM in tension were not quantified [14, 19, 27]. Compared to the lamella, the stiffness of the outer lamellae interface (i.e. ILM) was higher than the inner AF, (ranging between 43% to 75%).[28]. This result was consistent with a study indicating that AF peel strength was approximately 30% higher in outer lamellae compared to the inner layers [17].

While microstructural-based studies revealed that the density of elastic fibres were higher in the ILM compared to the lamellae [7-9, 12, 29, 30], ultrastructural studies provided new insights to the organization of elastic fibres in different regions of the disc [11, 31, 32]. A

dense network including thick (diameter of 1-2 μm) and thin (0.1 μm diameter) elastic fibres was seen in the ILM. This highly organised complex network was comprised of the majority of fibres oriented at ±45° to the circumferential lamellae, and having different size and shape fibres, compared to those in the intra-lamellar region [11].

Studies on the ILM were categorized into qualitative structural-based research where no mechanical measurement were undertaken [2, 11, 14, 19, 21, 29, 32], or quantitative research where a number of lamellae were used with limited mechanical properties reported [17, 18, 23, 28, 33]. While these studies have improved our knowledge of the possible mechanical role of the ILM, no studies have measured the viscoelastic and mechanical behaviour of the ILM under direct tensile and direct shear loading has not been studied, however peel tests, which would represent a more-tensile loading regime, have been performed.

Studies of multiple and single lamellae have demonstrated that these tissues exhibit increased modulus and failure stress with increasing strain rate, and a higher modulus in shear compared to tension [34] however no such studies have been conducted on the ILM. Therefore, the aim of this study was to measure the viscoelastic and failure properties of the ILM in both the tension and shear directions of loading. The following hypotheses were proposed:

1. The stiffness of the ILM will be significantly larger at faster strain rates, and energy absorption significantly smaller, compared to slower strain rates.

2. The viscoelastic and failure properties under tension and shear loading will not be significantly different.

The first hypothesis was proposed due to the combination of elastic fibres and extracellular matrix in the ILM, which most likely impart viscoelastic behaviour to the ILM. The second

hypothesis is based on the dominant orientation of elastic fibres at ±45°, which suggests a similar mechanical role in both tension and circumferential directions of loading.

2. Materials and methods:

2.1. Sample preparation

Sixteen Ovine spines (18-24 months old) were obtained from a local abattoir, and discs from lumbar FSUs (L4/L5) were dissected from vertebral bodies, sprayed with saline and stored at -20°C in cling wrap until used for sample preparation. While frozen, a 10 mm width of the anterior AF, with the depth to the nucleus pulposus region (~7mm disc height) was separated from each disc. Each AF tissue was moulded with optimal cutting temperature (OCT, Tissue-Tek®, Sakura, Japan) compound to identify the transverse cutting plane. Samples from adjacent sections (approximate thickness 1 mm and width 10 mm) were sliced using a hand microtome (Figure 1a-c). Damaged samples or those having less than ten lamellae were excluded from the study. All adjacent samples were labelled and then divided into two groups of 10 for mechanical testing in the radial (tension) and circumferential (shear) directions.

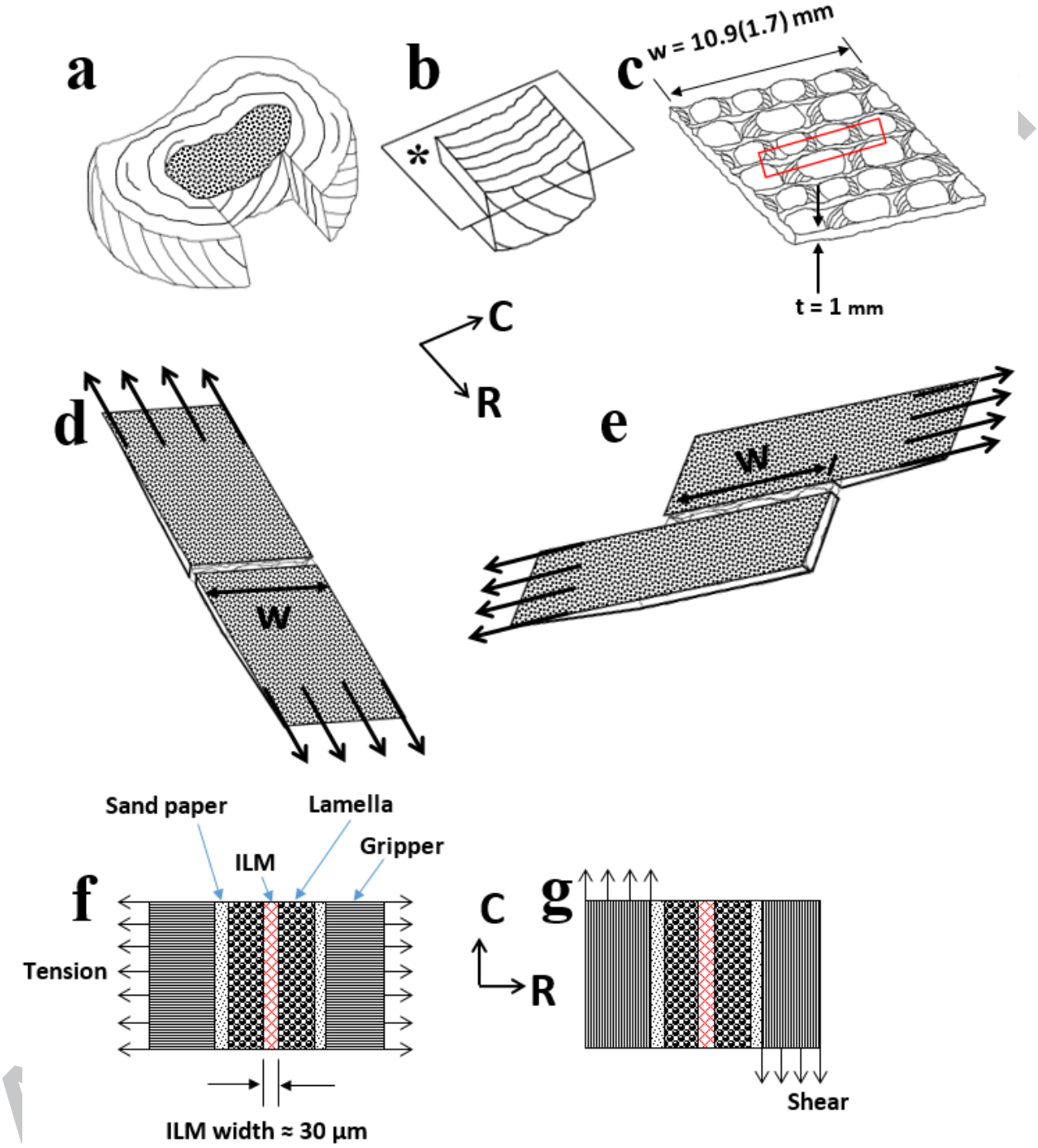

Figure 1. Sample preparation. (a) Anterior AF segments of approximately 10 mm width, were seperated from the outer AF to the nucleus pulposus, (b) frozen sections were then cut along the transverse plane (denoted by *), (c) transverse samples were sliced to approximately 1 mm thickness. The region identified by the red rectangle represents the approximate location from

which samples were prepared and tested. (d, e) samples of inter-lamellar matrix (ILM) and portions of two adjacent lamellae prepared for shear and tension tests, respectively. Sand paper was attached to the samples using superglue under microscope visualization (directions of applied load are identified by arrows). (f, g) schematic drawings of the samples from axial view to identify the size of the recruited adjacent lamellae compared to the ILM, where the width of the lamellae are greater than the ILM. The mean (95%CI) cross-sectional area of all samples was 10.9 (1.7) mm^2 as shown in (panel c). Axes R and C represent radial and circumferential directions, respectively, and dimension t and W indicate the specimen thickness and width, respectively.

2.2. Mechanical testing

To accomplish the ILM mechanical tests, a functional lamellae unit, which consisted of two adjacent lamellae and the ILM between them, was identified from prepared adjacent sections using a stereomicroscope (Motic, SMZ-168, China) (Figure 1d-e). The functional lamellae units were isolated from the middle of the AF (approximately 5-6 lamellae inwards) and was consistent for all samples. Previous ultrastructural studies identified an approximate 30 μm width for the ILM. During specimen preparation the total width of the lamella-ILM-lamella complex was approximately 200 μm and careful attention was used to ensure that the ILM was located in the middle of the complex. (Figure 1f -g). This strategy for sample preparation was consistent among all samples. Sand paper (250 grit) was bonded above and below the sample, and on each edge using cyanoacrylate adhesive. The mechanical properties of samples were measured in tension (radial) and shear (circumferential) loading directions.

Pilot failure mechanical tests for the ILM were performed at different strain magnitudes to identify the maximum strain (40%) used in this study, which was low enough (compared to the yield stress) to be non-destructive, yet high enough to include the linear region. The strain rate was estimated based on disc deformation data during compression from Costi et al., 2007

for the outer anterior radial AF displacement [35]. For every 1 mm of applied compressive displacement, the radial strain was 11%, as calculated between the two outermost anterior radial displacement vectors. In order to estimate the compressive displacement of the disc during physiological loading, an in-vivo nucleus pulposus pressure of 1.1 MPa that was measured during standing was used [36]. The equivalent axial compressive force [37]required to create the 1.1 MPa nucleus pressure was then calculated based on an average lumbar (L4-5) disc area of 2011 mm^2 [38], which yielded a compressive force of 1475 N. The resulting physiological compressive displacement was calculated to be 0.29 mm based on a compressive stiffness of normal discs of 5,141 N/mm taken from a loading frequency of 1 Hz [39]. Therefore, the radial strain for a compressive displacement of 0.29 mm was 3.2%. Using a sinusoidal physiological compressive loading frequency of 1 Hz, the peak outer anterior AF radial strain would be achieved in 0.5 s, which yields a strain rate of 6.4%/s. Based on this we chose a strain rate of 10 %/s, and then chose two other strain rates that were each an order of magnitude lower (1 %/s and 0.1 %/s).

All samples were initially equilibrated in 0.15M phosphate buffered saline (PBS) at room temperature for 30 min and immersed in 0.15M PBS at 37°C during tests. Each sample was subjected to dynamic and failure tests using a micromechanical testing machine (BioTester, CellScale, Waterloo, ON ,Canada) having a load cell capacity of 23 N. Prior to each test, a 100 mN preload was applied. Three cycles of dynamic loading using a triangle waveform were applied to stretch the samples to 40% of their initial length at three strain rates of $0.1\%s^{-1}$ (slow), $1\%s^{-1}$ (medium) and $10\%s^{-1}$ (fast) under displacement control, followed by a 5 min unloaded recovery period between each rate. Preload and recovery were used to minimise creep between tests. Data frequency acquisition was set to 1, 10 and 100 Hz for slow, medium and fast strain rates, respectively. Finally, a ramp test to failure was performed at a strain rate of $10\%s^{-1}$ at 100 Hz data acquisition.

2.3. Data and statistical analysis

Engineering stress and strain were calculated from the final cycle of the dynamic tests (Figure 2), and the failure test using custom-written MATLAB scripts (R2014b, The Mathworks Inc.). Outcome measures of phase angle, extensibility and modulus (toe, linear, average during entire load-unload cycle (average) and average during loading only (average loading)), were calculated from the dynamic tests, followed by the failure test parameters of failure stress and strain, and toughness. Failure stress was defined as the peak stress recorded during the test, and the corresponding strain was defined as the failure strain. All modulus measures were calculated as the slope of the best-fit line using linear regression. Toe modulus represented the initial region of the loading curve where the elastic fiber network in the ILM was uncoiling, and linear modulus represented the region where the majority of fibers in the ILM were fully recruited. Extensibility was calculated as the strain at the intersection of the toe and linear stiffness lines [40]. The average loading modulus represented the entire loading curve, and average modulus represented the entire load-unload curve. The phase angle, which is a measure of energy absorption, was calculated using a cross spectral density estimate function (MATLAB: csd.m) [39].

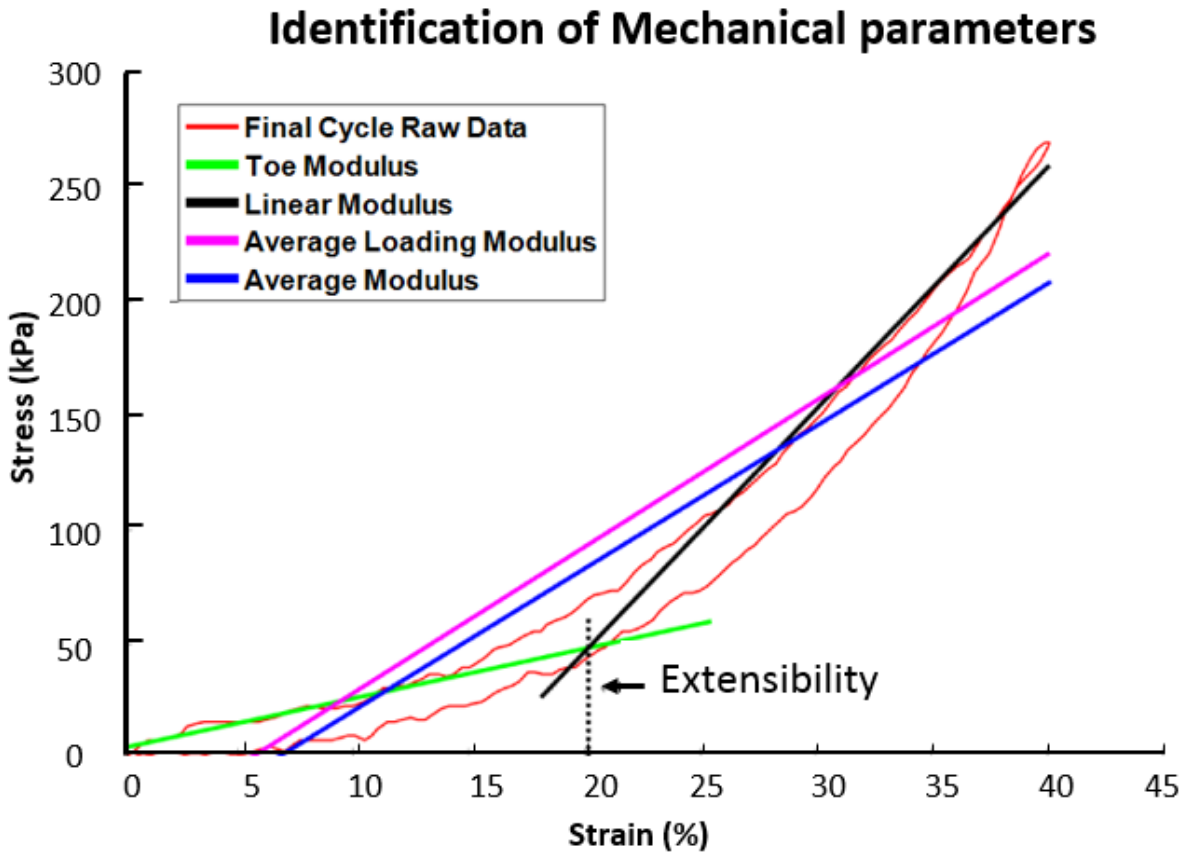

Figure 2- Identification of mechanical parameters including final cycle of data, extensibility, toe, linear, average loading and average moduli

For statistical analysis all data were assessed for normality using the Shapiro-Wilk test. For the dynamic test outcome parameters, separate repeated measures ANOVA were conducted (IBM SPSS Statistics for Windows, Version 22.0. Armonk, NY: IBM Corp.) for each variable of phase angle, extensibility, toe modulus, linear modulus and average modulus having fixed factors of direction of load application, (shear and tension), and strain rate ($0.1\%s^{-1}$ (slow), $1\%s^{-1}$ (medium) and $10\%s^{-1}$ (fast)) using an alpha of 0.05, with post-hoc multiple comparisons conducted using a Bonferroni adjustment on alpha. Statistical differences for ILM failure properties of failure stress, strain and toughness between tension and shear loadings were assessed using an unpaired t-test, using an alpha = 0.05.

3- Results

There was no indication of sample slippage during mechanical testing as identified from observation of the recorded video of each tests, and from the testing curves (Figure 3). Videos showing the failure of two different samples in tension and shear can be viewed in the supplementary information. The mean (95% CI) gripper to gripper distance was 1.172 (0.074) mm. The dimensions of the samples were approximately a thickness of 1 mm, a width of 10.9 (1.7) mm. When tested to failure, all samples failed at the ILM site. According to the Shapiro-Wilk test, it was found that the data for all specimens were normally distributed ($p > 0.05$).

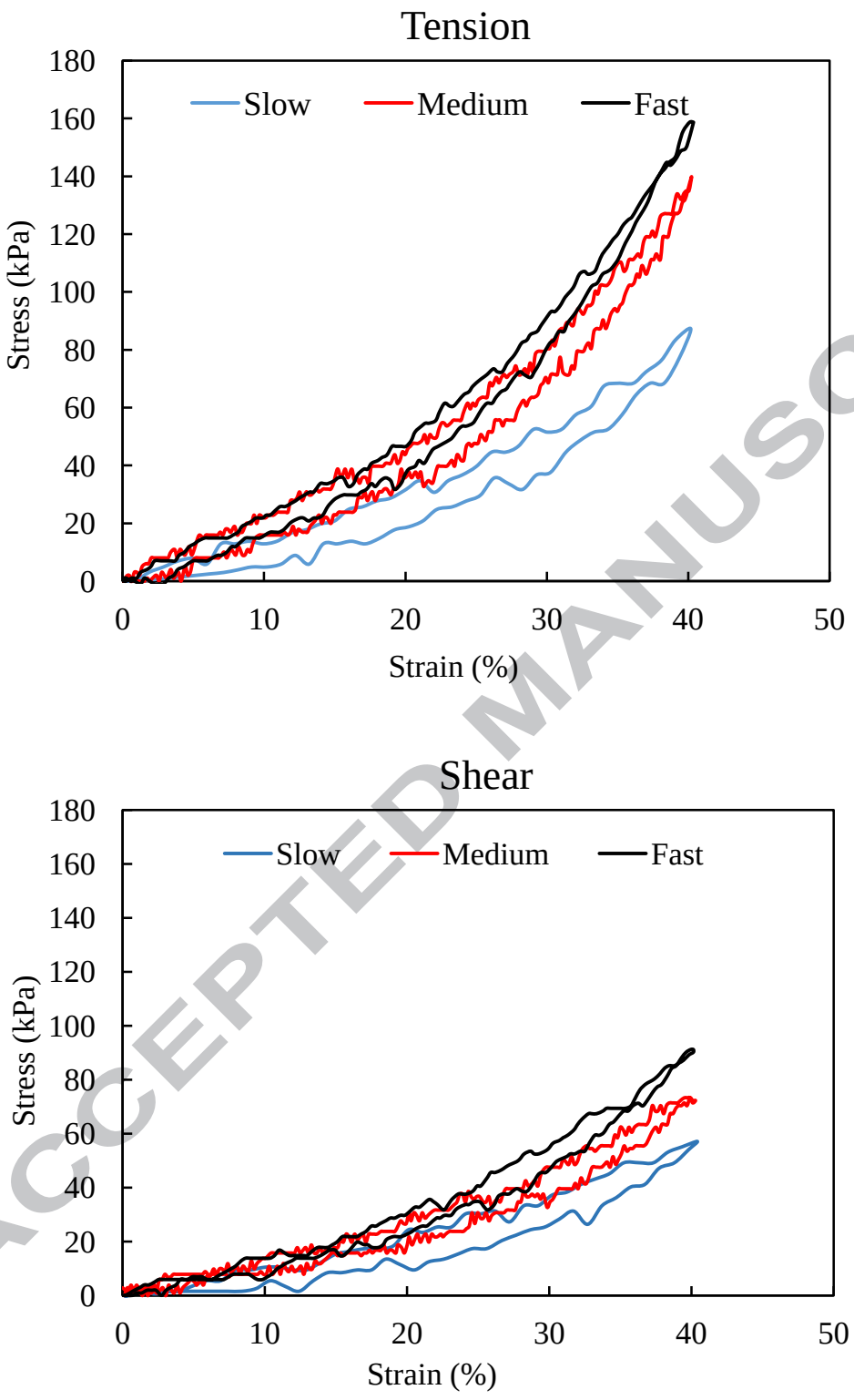

Figure 3- The viscoelastic properties (final loading cycle) of the ILM for the same sample tested at three different strain rates of 0.1%s^{-1} (slow), 1%s^{-1} (medium) and

10%s^{-1} (fast) in (a) radial (tension) and for a second sample tested in (b) circumferential (shear) .

Statistical analysis for phase angle, extensibility, average modulus, toe modulus, linear modulus, and average loading modulus are reported as follows:

Phase angle

The overall effect of strain rate was significant ($p < 0.001$, Table 1), with post-hoc comparisons revealing a significantly larger phase angle at slow compared to the medium and fast strain rates ($p < 0.001$, Figure 4a). The overall effect of loading direction (tension vs. shear) and the interaction between strain rate and loading direction was not significant ($p = 0.226$ and $p = 0.545$ respectively).

Extensibility

No significant overall effects were found for strain rate ($p = 0.631$), or loading direction ($p = 0.574$) for extensibility, nor their interactions ($p = 0.442$), (Table 1, Figure 4b).

Average modulus

The overall effects of strain rate ($p = 0.173$) and loading direction ($p = 0.110$) for average modulus, was not significant, nor their interactions ($p = 0.417$), (Table 1, Figure 4c).

Average loading modulus

The overall effect of strain rate was significant for average loading modulus ($p = 0.017$, Table 1), with post-hoc comparisons revealing that the slow strain rate was significantly smaller compared to fast ($p = 0.05$, Figure 4d). No significant difference was found between slow and medium ($p = 0.191$) as well as between fast and medium ($p = 0.069$) strain rates. A trend of larger modulus at higher stain rates was seen for the effect of loading direction on average

loading modulus (p = 0.051). No significant interactions between strain rate and loading direction were found (p = 0.797).

Toe modulus

The overall effect of strain rate was significant for toe modulus (p = 0.005, Table 1), with post-hoc comparisons revealing a significantly larger toe modulus for the fast strain rate compared to medium (p = 0.019, Figure 4e) and slow (p = 0.035). No significant difference for toe modulus was found between slow and medium strain rates (p = 0.098). Also the overall effect of loading direction was significant for toe modulus (p = 0.046), with post-hoc comparisons revealing that toe modulus was significantly smaller in shear compared to tension (p =0.046). No significant interaction was found between strain rate and loading direction (p = 0.779).

Linear modulus

The overall effect of strain rate was not significant for linear modulus (p = 0.061, Table 1). The overall effect of loading direction was significant (p = 0.009) for linear modulus, with post-hoc comparisons revealing that the tension group was significantly larger than the shear group (p = 0.004). No significant interactions were found between strain rate and loading direction (p = 0.681) (Figure 4f).

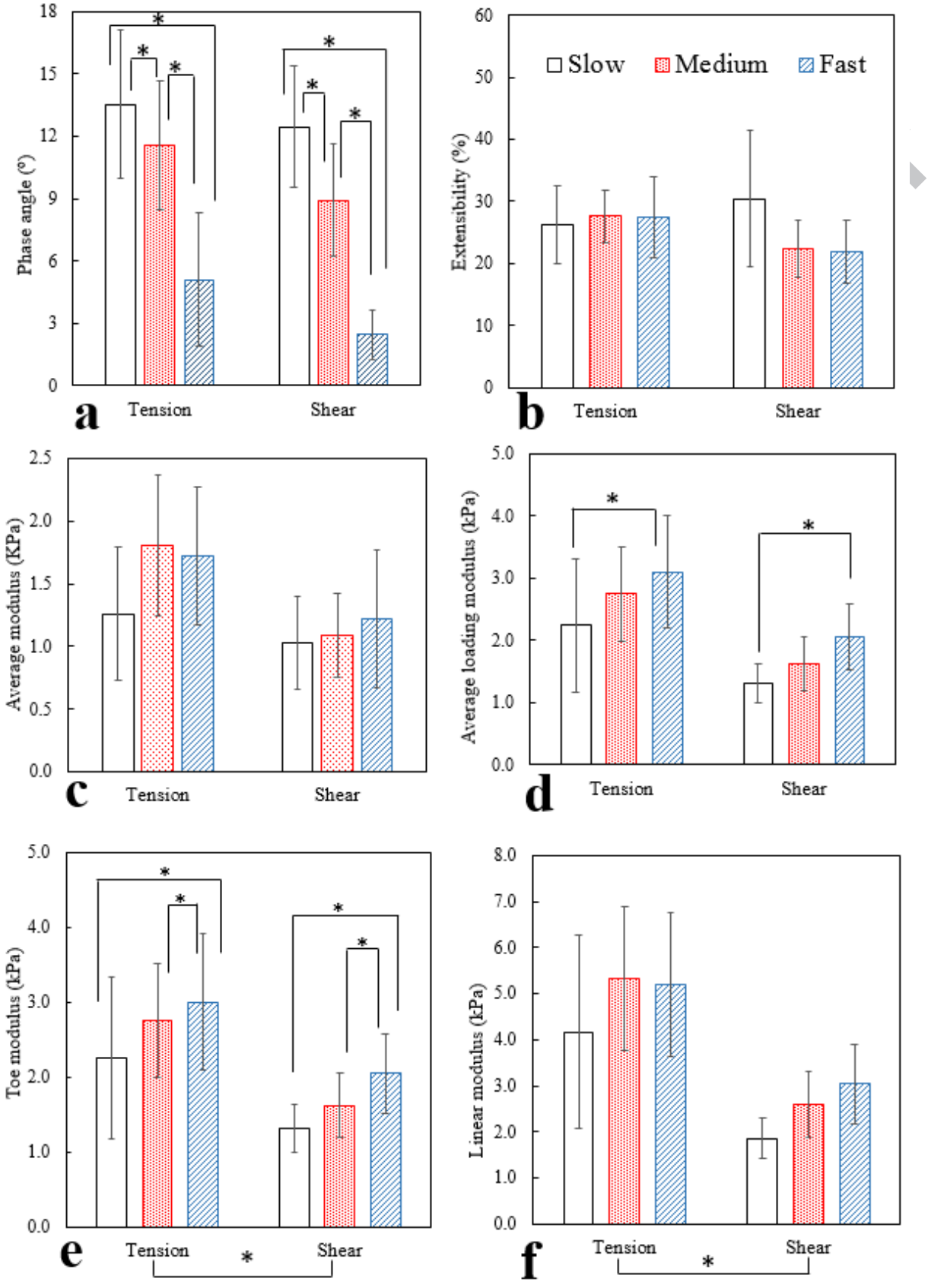
Phase angle (°)
18
15
12
9
6
3
0
*
*
*
*
*
*
a
Tension
Shear
Extensibility (%)
60
50
40
30
20
10
0
Slow
Medium
Fast
b
Tension
Shear
Average modulus (KPa)
2.5
2.0
1.5
1.0
0.5
0.0
c
Tension
Shear
Average loading modulus (kPa)
5.0
4.0
3.0
2.0
1.0
0.0
*
*
d
Tension
Shear
Toe modulus (kPa)
5.0
4.0
3.0
2.0
1.0
0.0
*
*
*
*
e
Tension
*
Shear
Linear modulus (kPa)
8.0
7.0
6.0
5.0
4.0
3.0
2.0
1.0
0.0
f
Tension
*
Shear

Figure 4- Comparison of selected mechanical properties of the ILM at three strain rates of 0.1%s^{-1} (slow), 1%s^{-1} (medium) and 10%s^{-1} (fast), during tension and shear loading (a) Phase angle, (b) Extensibility, (c) Average modulus, (d) Average loading modulus, (e) Toe modulus and (f) Linear modulus. * denotes significant differences between groups.

Failure tests

Loading direction (tension and shear) was not significant for failure stress (p = 0.674), failure strain (p = 0.341) and toughness (p = 0.366) (Figure 5). The mean (95%CI) ILM toughness was 0.54 (0.22) and 0.79 (0.48) J.m^{-3}, in tension and shear directions, respectively, which was not significant (p = 0.366).

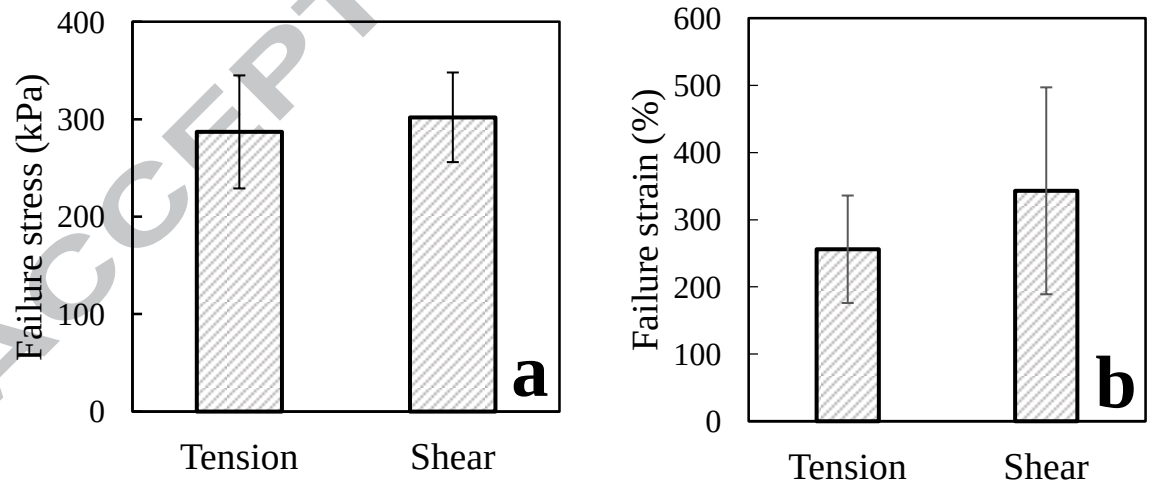

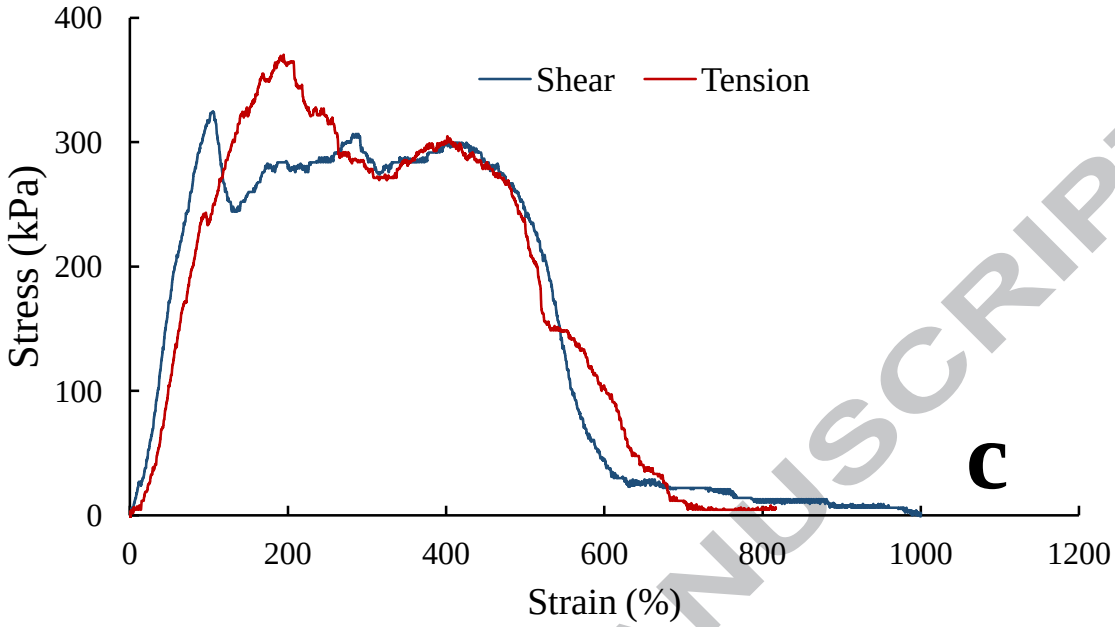

Figure 5- Comparison of mean (95%CI) (a) Failure stress and (b) Failure strain of the ILM in tension and shear loading directions. (c) Example stress-strain failure curves during shear and tension loading of the ILM in adjacent samples from the same disc.

Table 1. Summary of ANOVA results for the overall effects of strain rate (slow vs. medium vs. fast) and loading direction (tension vs. shear) and their interactions for each of the micro-mechanical test parameters. The * symbol and NSD were used to indicate significant and no significant difference, respectively.

Parameter	Strain rate	Loading direction	Interactions
Phase Angle (°)	*($p < 0.001$)	NSD ($p = 0.226$)	NSD ($p = 0.545$)
Extensibility (%)	NSD ($p = 0.631$)	NSD ($p = 0.574$)	NSD ($p = 0.442$)
Average Modulus (kPa)	NSD ($p = 0.173$)	NSD ($p = 0.110$)	NSD ($p = 0.417$)
Average Loading Modulus (kPa)	*($p = 0.017$)	NSD ($p = 0.051$)	NSD ($p = 0.797$)
Toe Modulus (kPa)	*($p = 0.005$)	*($p = 0.046$)	NSD ($p = 0.779$)
Linear Modulus (kPa)	NSD ($p = 0.061$)	*($p = 0.009$)	NSD ($p = 0.681$)

4- Discussion

Understanding the mechanical function of the ILM is an important step towards developing more accurate multi-scale computational models for disc function, which can lead to

improved strategies for tissue engineering and repair. The aim of this study was to measure, for the first time, the viscoelastic and failure material properties of the ILM under tension and shear loading. The findings from this study confirmed both of our hypotheses that the stiffness of the ILM was significantly larger at faster strain rates, and energy absorption significantly smaller, compared to slower strain rates, and the viscoelastic and failure properties were not significantly different under tension and shear loading. We found a strain rate dependent response of the ILM during dynamic loading, particularly at the fastest rate. The ILM demonstrated a significantly higher capability for energy absorption, as measured by phase angle, at slow strain rates compared to medium and fast strain rates. A significant increase in modulus was found in both loading directions and all strain rates, having a trend of larger modulus in tension and at faster strain rates. It was revealed that average loading modulus in tension was marginally non-significant compared to shear ($p = 0.051$), while it seems with increasing the number of specimens it become significant. The overall interaction between loading direction and strain rate was not significant for all viscoelastic parameters. When tested to failure, there were no significant differences in failure stress, strain and toughness between ILM tensile and shear loading directions.

The recorded videos during the failure and viscoelastic tests in different directions of loading (supplementary files) provide additional detail of where and how the lamella-ILM-lamella complex fails. Also, the images at different time points during tension (Figure 6) and shear (Figure 7) tests provide more information for the role of the ILM in the AF during loading in different directions. Time was presented on the abscissa instead of strain, to allow for a direct comparison to the videos in the supplementary files. While it was not possible, at this magnification, to observe the likely sub-failure of the samples that occurred in both directions of loading after 2 s (Figures 6b and 7b) to the peak stress (denoted by c), the failure was more likely to commence at peak stress (Figures 6c and 7c). The observed fluctuation for stress

after the linear region to the peak stress (point b to c), which were seen to be less that those after initiation of failure and its propagation (point c to e), may represent the changes in ultrastructural organization of the elastic fibers in the ILM, which may arise from the expansion of the elastic fiber network, rotation of fibers, separation between ECM and elastic fiber network and the failure of the thin elastic fibers. The observed fluctuations after initiation of failure (Figure 6c, 7c) to the point of separation of the lamellae (Figure 6e, 7e) may represent the failure of the thick elastic fibers in the ILM.

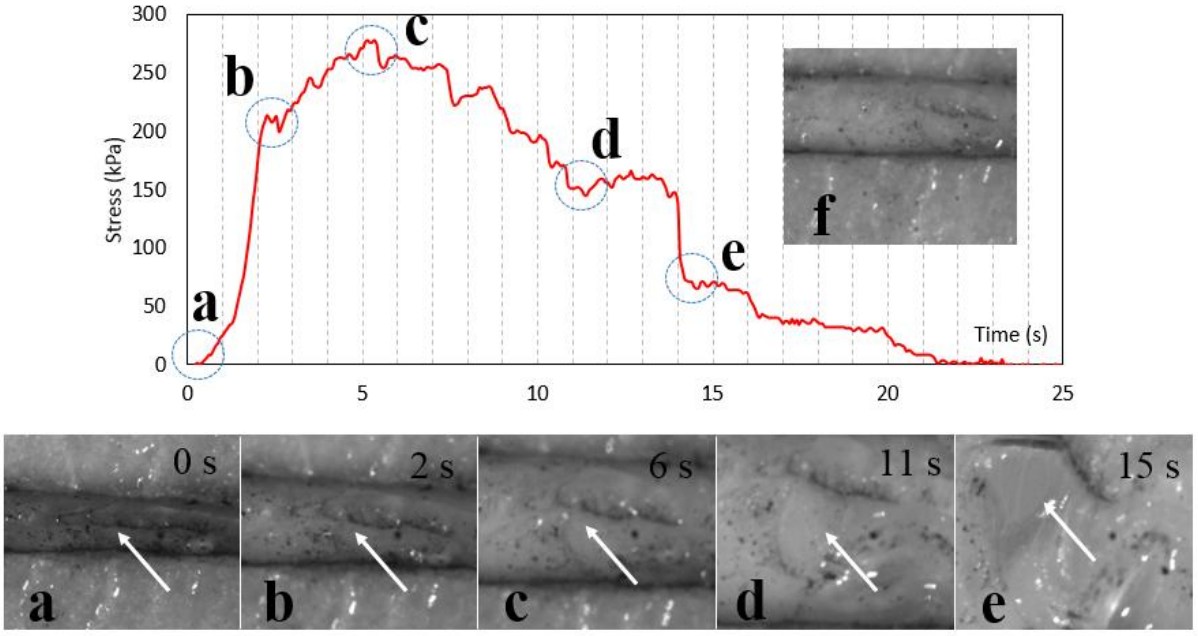

Figure 6 - Change in stress during the performance of mechanical failure for the ILM in tension. (a, b and c) represent rest point, yield stress and maximum stress, respectively and (d, e) indicate the ILM disruption and separation, respectively. The correspondence images show the change in the appearance of the samples during mechanical failure test at different time points (seconds) as indicated in the graph. (f) Represents the sample after stretched to 40% of its initial length. Arrows indicate the approximate location of the ILM in the middle of lamella-ILM-lamella complex (a, b) and initiation (c), propagation (d) of the failure as well as (e) the lamella separation.

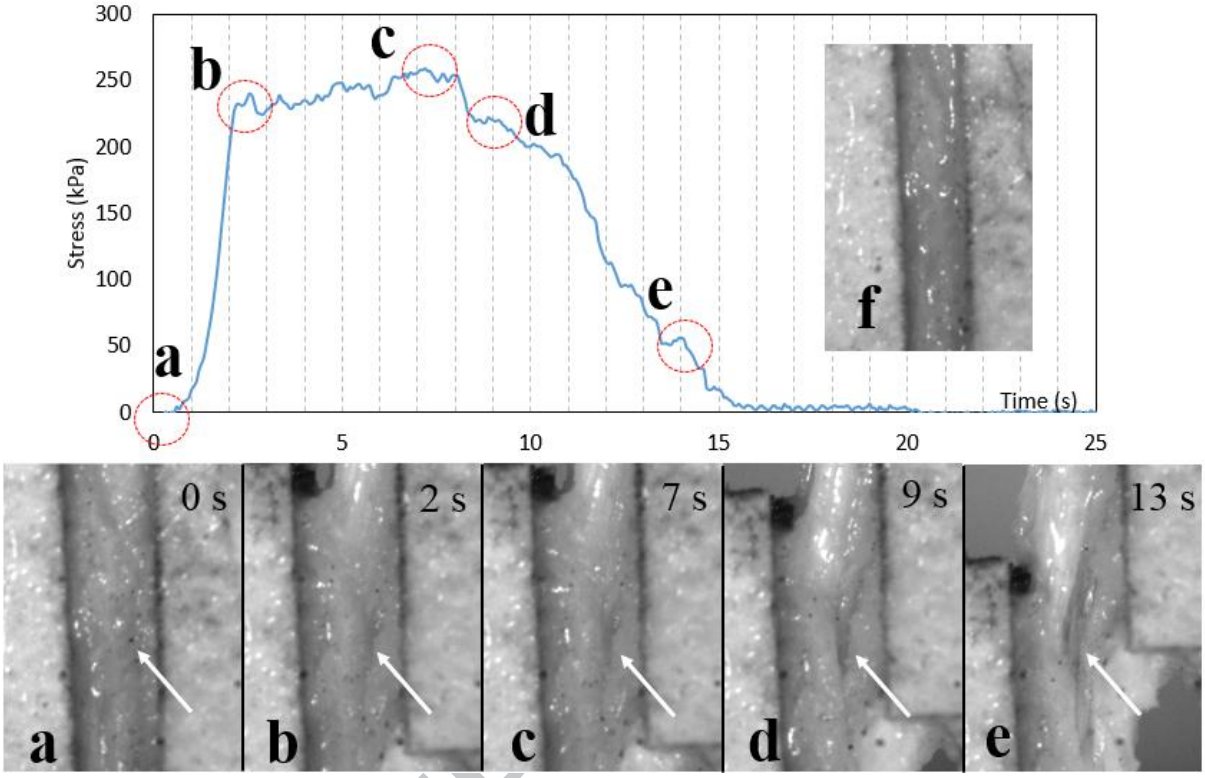

Figure 7 - The stress-time curve during the performance of mechanical failure for the ILM in shear. (a, b and c) represent rest point, yield stress and maximum stress, respectively and (d, e) indicate the ILM disruption and separation, respectively. The correspondence images show the change in the appearance of the samples during mechanical failure test at different time points (seconds) as indicated in the graph. (f) Represents the sample after stretched to 40% of its initial length. Arrows indicate the approximate location of the ILM in the middle of lamella-ILM-lamella complex (a, b) and initiation (c), propagation (d) of the failure as well as (e) the lamella separation.

Failure of the lamella-ILM-lamella complex more likely occurred at the ILM site, where the looser network of elastic fibers was present compared to the lamella having dense and highly packed collagen bundles. The lower stiffness of the ILM, together with the orthotropic

ultrastructure, suggests a role that is adapted to support 6 degree of freedom deformation of the AF, and absorb more energy than the lamellae.

Our ultrastructural studies of the elastic fiber network in the ILM revealed that the dominant elastic fiber orientation, relative to the circumferential (lamellae) direction, was near 0°, with two symmetrical peaks of approximately ±45°, indicating the presence of an orthotropic structure [11]. This structure likely explains why a lower modulus (toe, linear and average) was found in shear compared to tension, where only those fibers oriented in the direction of applied shear would be recruited. We identified the presence of both thick and thin elastic fibers, with the thicker fibers aligned parallel to the lamellae [11, 31]. It may be that in shear, the thicker fibers experienced the highest stresses and failed first, as observed by the abrupt decrease in stress (Figures 5c, 6 and 7), followed by the thinner fibers taking up the stress and progressively failing. In tension, the network of "crossing" fibers (±45°) were likely all recruited, after which they failed sequentially, resulting in a less abrupt decrease in stress. Based on protein-proteoglycan interactions, supramolecular assemblies (elastic fibers, collagen fibrils) are formed and a structural scaffold is provided by ECM. The mechanical entanglement and binding of this structural scaffold with elastic fibers in the ILM, provides a structurally stable composite, contributing to the mechanical properties of the ILM, which likely to plays an important role in imparting isotropic failure properties [41].

Unfortunately, few studies have been undertaken to identify the role of the ILM on mechanical properties of the AF. The observations implying that the ILM was mainly composed of elastic fibres [2, 9, 10, 29], having an overall low density relative to collagen fibres [42], may address why such studies are lacking. Therefore, comparisons to other studies is limited. The findings of this study strongly support the previous reports that suggested a biomechanical role for the ILM based on the observation of alignment of collagen and elastic fibers after loading [27, 43], and a well-organized ultra-structural

arrangement of the elastic fiber network [11]. Only one study has reported human ILM failure strength as a peel strength of 18.4 kPa in the anterior region of degenerated discs (grade 3, [17]), which is an order of magnitude lower than our non-degenerated ovine disc with a mean (95%CI) tension strength of 287 (58) kPa. In addition, the mean (SD) peel strength (normalized to the sample width) of the rabbit ILM was reported to be 0.88 (0.26) N/mm that can compared to the peak tension force (normalized by width) in our study measured as mean (SD) 0.28 (0.093) N/mm. The peak load for delamination of the AF measured by a lap test using porcine cervical discs was reported to be mean (SD) 0.3 (0.02) N/mm, compared to our normalized ovine shear maximum force of 0.396 (0.22) N/mm at the anterior region [18, 23]. From another point of view, based on the results of this study we are able to compare the mechanical properties of the ILM to those of the lamellae. The AF lamella shear failure strength (strain rate: 2 $\%s^{-1}$) was reported as 1.03 ± 0.85 MPa in porcine cervical discs [44], and our measurement showed that the ILM tensile and shear failure strengths were 0.29 (0.58) MPa and 0.30 (0.46) MPa, respectively (Figure 5a). These comparisons indicate that ILM material properties are comparable to that of the lamellae, which presents evidence in support of the key role of the ILM on mechanical properties of the AF in the disc.

Calculating strain using gripper-to-gripper distance, instead of utilizing a non-contact method, presents a limitation, however since there was no evidence of sample slippage, the measured strain is representative of global tissue strain. While it is un-likely that the strain is constant across the ILM, the calculation of the ILM strain may be affected by the presence of adjacent lamellae and therefore represents the global strain across the ILM and ILM-lamella boundary. However, our studies have found that ILM has a significantly lower failure stress compared to the adjacent lamellae, indicate that the ILM is weaker (unpublished data). From a structural point of view, the lamella consists of dense and highly packed collagen fibers,

while elastic fibers are a looser network within the ILM. Another limitation of this study was the use of an ovine model. There is strong evidence that supports the use of an ovine model based on its structural and biochemical similarities to the human disc [19-21, 28, 45-50]; however, using human samples would be more clinically relevant. While it is likely that the mechanical properties of the ILM in tension and shear directions of loading are not the same in different regions of the disc, the use of only the anterior region was a limitation of this study. The preparation of adjacent samples from other regions in ovine discs was difficult due to the small disc height; however, different regions could readily be isolated in human discs. Also we acknowledge that using isolated ILM samples, despite its preparation being challenging, was important for minimizing the lamellae contribution to mechanical properties.

5. Conclusion

This study identified the mechanical contribution of the ILM to the structural integrity of the AF, in both tension and shear directions of loading. The strain rate dependent response of the ILM during dynamic loading and its significantly higher capability for energy absorption at slow strain rates in both directions of loading, confirmed its viscoelastic behavior. More importantly, the finding of no significant difference in failure properties in both loading directions, was consistent with our previous ultra-structural studies that revealed a well-organized (±45°) elastic fibre orientation in the ILM. The results from this study can be used to develop and validating finite element models of the AF at the tissue scale, as well as providing new strategies for fabricating tissue engineered scaffolds. This research will serve as a foundation for future studies on the relationship between degeneration and ILM mechanical properties, as well as understanding the contribution of the elastic fibre network to the mechanical properties of the ILM.

6- References

[1] J.J. Cassidy, A. Hiltner, E. Baer, Hierarchical structure of the intervertebral disc, Connective tissue research 23(1) (1989) 75-88.
[2] J. Tavakoli, D.M. Elliott, J.J. Costi, Structure and mechanical function of the inter-lamellar matrix of the annulus fibrosus in the disc, Journal of orthopaedic research : official publication of the Orthopaedic Research Society 34(8) (2016) 1307-15.
[3] J. Melrose, S.M. Smith, R.C. Appleyard, C.B. Little, Aggrecan, versican and type VI collagen are components of annular translamellar crossbridges in the intervertebral disc, Eur Spine J 17(2) (2008) 314-324.
[4] S.B. Bruehlmann, J.B. Rattner, J.R. Matyas, N.A. Duncan, Regional variations in the cellular matrix of the annulus fibrosus of the intervertebral disc, J Anat 201(2) (2002) 159-71.
[5] E.F. Johnson, K. Chetty, I.M. Moore, A. Stewart, W. Jones, The distribution and arrangement of elastic fibres in the intervertebral disc of the adult human, J Anat 135(Pt 2) (1982) 301-9.
[6] J.A. Buckwalter, R.R. Cooper, J.A. Maynard, Elastic fibers in human intervertebral discs, The Journal of Bone & Joint Surgery 58(1) (1976) 73.
[7] L.J. Smith, N.L. Fazzalari, Regional variations in the density and arrangement of elastic fibres in the anulus fibrosus of the human lumbar disc, J Anat 209(3) (2006) 359-367.
[8] L.J. Smith, N.L. Fazzalari, The elastic fibre network of the human lumbar anulus fibrosus: architecture, mechanical function and potential role in the progression of intervertebral disc degeneration, Eur Spine J 18(4) (2009) 439-48.
[9] J. Yu, C. Peter, S. Roberts, J.P. Urban, Elastic fibre organization in the intervertebral discs of the bovine tail, J Anat 201(6) (2002) 465-475.
[10] J. Yu, U. Tirlapur, J. Fairbank, P. Handford, S. Roberts, C.P. Winlove, Z. Cui, J. Urban, Microfibrils, elastin fibres and collagen fibres in the human intervertebral disc and bovine tail disc, J Anat 210(4) (2007) 460-471.
[11] J. Tavakoli, D.M. Elliott, J.J. Costi, The ultra-structural organization of the elastic network in the intra- and inter-lamellar matrix of the intervertebral disc, Acta Biomater 58 (2017) 269-277.
[12] J. Yu, J.C. Fairbank, S. Roberts, J.P. Urban, The elastic fiber network of the anulus fibrosus of the normal and scoliotic human intervertebral disc, Spine 30(16) (2005) 1815-20.
[13] J.P. Urban, S. Roberts, Degeneration of the intervertebral disc, Arthritis research & therapy 5(3) (2003) 120-30.
[14] C.A. Pezowicz, P.A. Robertson, N.D. Broom, The structural basis of interlamellar cohesion in the intervertebral disc wall, J Anat 208(3) (2006) 317-330.
[15] S.H. Lee, R. Derby, Y. Chen, K.S. Seo, M.J. Kim, In vitro measurement of pressure in intervertebral discs and annulus fibrosus with and without annular tears during discography, The spine journal : official journal of the North American Spine Society 4(6) (2004) 614-8.
[16] O.L. Osti, B. Vernonroberts, R. Moore, R.D. Fraser, Annular Tears and Disk Degeneration in the Lumbar Spine - a Postmortem Study of 135 Disks, J Bone Joint Surg Br 74(5) (1992) 678-682.
[17] D.E. Gregory, W.C. Bae, R.L. Sah, K. Masuda, Anular delamination strength of human lumbar intervertebral disc, Eur Spine J 21(9) (2012) 1716-1723.
[18] D.E. Gregory, W.C. Bae, R.L. Sah, K. Masuda, Disc degeneration reduces the delamination strength of the annulus fibrosus in the rabbit annular disc puncture model, The Spine Journal 14(7) (2014) 1265-1271.
[19] S.P. Veres, P.A. Robertson, N.D. Broom, ISSLS Prize Winner: Microstructure and Mechanical Disruption of the Lumbar Disc Annulus Part II: How the Annulus Fails Under Hydrostatic Pressure, Spine 33(25) (2008) 2711-2720.
[20] N.L. Fazzalari, J.J. Costi, T.C. Hearn, R.D. Fraser, B. Vernon-Roberts, J. Hutchinson, B.A. Manthey, I.H. Parkinson, C. Sinclair, Mechanical and Pathologic Consequences of Induced Concentric Anular Tears in an Ovine Model, Spine 26(23) (2001) 2575-2581.

[21] M.L. Schollum, P.A. Robertson, N.D. Broom, ISSLS Prize Winner: Microstructure and Mechanical Disruption of the Lumbar Disc Annulus Part I: A Microscopic Investigation of the Translamellar Bridging Network, Spine 33(25) (2008) 2702-2710.
[22] J.C. Iatridis, I. ap Gwynn, Mechanisms for mechanical damage in the intervertebral disc annulus fibrosus, Journal of biomechanics 37(8) (2004) 1165-1175.
[23] D.E. Gregory, J.H. Veldhuis, C. Horst, G. Wayne Brodland, J.P. Callaghan, Novel lap test determines the mechanics of delamination between annular lamellae of the intervertebral disc, Journal of biomechanics 44(1) (2011) 97-102.
[24] K.M. Labus, S.K. Han, A.H. Hsieh, C.M. Puttlitz, A Computational Model to Describe the Regional Interlamellar Shear of the Annulus Fibrosus, J Biomech Eng-T Asme 136(5) (2014).
[25] N.T. Hollingsworth, D.R. Wagner, Modeling shear behavior of the annulus fibrosus, J Mech Behav Biomed Mater 4(7) (2011) 1103-14.
[26] C. Vergari, J. Mansfield, J.R. Meakin, P.C. Winlove, Lamellar and fibre bundle mechanics of the annulus fibrosus in bovine intervertebral disc, Acta Biomater 37 (2016) 14-20.
[27] C.A. Pezowicz, P.A. Robertson, N.D. Broom, Intralamellar relationships within the collagenous architecture of the annulus fibrosus imaged in its fully hydrated state, J Anat 207(4) (2005) 299-312.
[28] M. Mengoni, B.J. Luxmoore, V.N. Wijayathunga, A.C. Jones, N.D. Broom, R.K. Wilcox, Derivation of inter-lamellar behaviour of the intervertebral disc annulus, J Mech Behav Biomed 48 (2015) 164-172.
[29] J. Yu, M.L. Schollum, K.R. Wade, N.D. Broom, J.P. Urban, ISSLS Prize Winner: A Detailed Examination of the Elastic Network Leads to a New Understanding of Annulus Fibrosus Organization, Spine 40(15) (2015) 1149-57.
[30] J. Yu, Elastic tissues of the intervertebral disc, Biochemical Society transactions 30(Pt 6) (2002) 848-52.
[31] J. Tavakoli, J. Costi, Ultrastructural organization of elastic fibres in the partition boundaries of the annulus fibrosus within the intervertebral disc Acta Biomater (Accepted) (2017).
[32] J. Tavakoli, J.J. Costi, Development of a rapid matrix digestion technique for ultrastructural analysis of elastic fibers in the intervertebral disc, J Mech Behav Biomed 71 (2017) 175-183.
[33] J.C. Iatridis, S. Kumar, R.J. Foster, M. Weidenbaum, V.C. Mow, Shear mechanical properties of human lumbar annulus fibrosus, J Orthopaed Res 17(5) (1999) 732-737.
[34] N. Newell, J.P. Little, A. Christou, M.A. Adams, C.J. Adam, S.D. Masouros, Biomechanics of the human intervertebral disc: A review of testing techniques and results, J Mech Behav Biomed 69 (2017) 420-434.
[35] J.J. Costi, I.A. Stokes, M. Gardner-Morse, J.P. Laible, H.M. Scoffone, J.C. Iatridis, Direct measurement of intervertebral disc maximum shear strain in six degrees of freedom: motions that place disc tissue at risk of injury, Journal of biomechanics 40(11) (2007) 2457-66.
[36] H.J. Wilke, P. Neef, M. Caimi, T. Hoogland, L.E. Claes, New in vivo measurements of pressures in the intervertebral disc in daily life, Spine 24(8) (1999) 755-62.
[37] A. Nachemson, J.M. Morris, In vivo measurements of intradiscal pressure. Discometery, a method for the determination of pressure in the lower lumbar disc, J bone and joint surg. American volume 46 (1964) 1077-92.
[38] D.B. Amin, D. Sommerfeld, I.M. Lawless, R.M. Stanley, B. Ding, J.J. Costi, Effect of degeneration on the six degree of freedom mechanical properties of human lumbar spine segments, J Orthopaed Res 34(8) (2016) 1399-1409.
[39] J.J. Costi, I.A. Stokes, M.G. Gardner-Morse, J.C. Iatridis, Frequency-Dependent Behavior of the Intervertebral Disc in Response to Each of Six Degree of Freedom Dynamic Loading: Solid Phase and Fluid Phase Contributions, Spine 33(16) (2008) 1731-1738.
[40] D.T. Pham, J.G. Shapter, J.J. Costi, Tensile behaviour of individual fibre bundles in the human lumbar anulus fibrosus, Journal of biomechanics 67 (2018) 24-31.
[41] B. Yue, Biology of the Extracellular Matrix: An Overview, Journal of glaucoma (2014) S20-S23.

[42] E.F. Johnson, H. Berryman, R. Mitchell, W.B. Wood, Elastic fibres in the anulus fibrosus of the adult human lumbar intervertebral disc. A preliminary report, J Anat 143 (1985) 57-63.
[43] W.M. Han, S.J. Heo, T.P. Driscoll, L.J. Smith, R.L. Mauck, D.M. Elliott, Macro- to Microscale Strain Transfer in Fibrous Tissues is Heterogeneous and Tissue-Specific, Biophys J 105(3) (2013) 807-817.
[44] D.E. Gregory, J.P. Callaghan, Does Vibration Influence the Initiation of Intervertebral Disc Herniation?: An Examination of Herniation Occurrence Using a Porcine Cervical Disc Model, Spine 36(4) (2011) E225-E231.
[45] H.-J. Wilke, A. Kettler, L.E. Claes, Are sheep spines a valid biomechanical model for human spines?, Spine 22(20) (1997) 2365-2374.
[46] G.D. O'connell, E.J. Vresilovic, D.M. Elliott, Comparison of animals used in disc research to human lumbar disc geometry, Spine 32(3) (2007) 328-333.
[47] M.L. Schollum, P.A. Robertson, N.D. Broom, A microstructural investigation of intervertebral disc lamellar connectivity: detailed analysis of the translamellar bridges, J Anat 214(6) (2009) 805-816.
[48] M.L. Schollum, P.A. Robertson, N.D. Broom, How age influences unravelling morphology of annular lamellae - a study of interfibre cohesivity in the lumbar disc, J Anat 216(3) (2010) 310-319.
[49] S.P. Veres, P.A. Robertson, N.D. Broom, ISSLS prize winner: how loading rate influences disc failure mechanics: a microstructural assessment of internal disruption, Spine 35(21) (2010) 1897-1908.
[50] S.P. Veres, P.A. Robertson, N.D. Broom, The influence of torsion on disc herniation when combined with flexion, Eur Spine J 19(9) (2010) 1468-1478.